scientific reports

OPEN

Design of a plasmonic optical biosensor based on a metal-insulator-metal ring resonator for the detection of various bacterial pathogens

Ali Khodaie, Yousef Rafighirani, Hamid Heidarzadeh✉ & Javad Javidan

Rapid and sensitive detection of pathogenic bacteria is essential for healthcare, food safety, and environmental monitoring. However, conventional detection techniques often fall short in terms of the speed and sensitivity required for real-time applications. In this study, we propose a label-free plasmonic optical biosensor based on a metal–insulator–metal (MIM) dual-ring resonator structure for the efficient detection of bacterial species. The sensor geometry was optimized using Particle Swarm Optimization (PSO) and evaluated through three-dimensional finite-difference time-domain (3D-FDTD) simulations to enhance both sensitivity and figure of merit (FOM). Gold nanorings integrated with a gold back reflector were employed due to their superior plasmonic resonance characteristics. The optimized design achieved a sensitivity of 324.76 nm·RIU^{-1}, a FOM of 10.187 RIU^{-1}, and a detection limit (LoD) of 0.075 RIU. The biosensor maintained high performance under varying operational conditions, including temperature (0–500 K), incident angle (0°–50°), and polarization states. Strong field confinement in the dielectric gap significantly enhanced the interaction between light and the analyte. The device demonstrated the ability to detect and differentiate between Vibrio cholerae (*n* = 1.365), Escherichia coli (*n* = 1.388), and Pseudomonas species (*n* = 1.437–1.526), highlighting its potential for quantitative bacterial identification. By addressing key limitations in sensitivity and specificity in complex biological environments, this MIM-based sensor offers a robust platform for rapid, high-throughput bacterial detection in clinical diagnostics and beyond.

Keywords Optical biosensor, Sensitivity, Bacteria, MIM resonator rings

The rapid detection of pathogenic bacteria is a critical challenge in modern healthcare, food safety, and environmental monitoring. Bacterial infections remain a leading cause of morbidity and mortality worldwide, with delays in diagnosis often exacerbating clinical outcomes[1]. Traditional bacterial detection methods, such as microbial culture, polymerase chain reaction (PCR), and enzyme-linked immunosorbent assays (ELISA), have long been the gold standard due to their reliability and specificity[2]. However, these techniques suffer from significant drawbacks, including lengthy processing times, the requirement for specialized laboratory infrastructure, and the need for skilled personnel[3]. These limitations render them impractical for point-of-care (PoC) applications or real-time monitoring, particularly in resource-limited settings where rapid and accessible diagnostics are most needed[4]. Moreover, their sensitivity is often insufficient to detect bacterial presence at early stages of infection, further highlighting the need for innovative alternatives[5]. In recent years, optical biosensors have emerged as a transformative technology to address these challenges, offering label-free detection, real-time analysis, and the potential for miniaturization[6]. Among these, plasmonic biosensors have gained significant attention due to their exceptional sensitivity to changes in the local refractive index, a property driven by the excitation of surface plasmon polaritons (SPPs) at metal-dielectric interfaces[7]. SPPs are electromagnetic waves that propagate along the boundary between a metal and a dielectric, exhibiting strong field confinement beyond the diffraction limit[8]. This confinement enhances light-matter interactions, making plasmonic sensors highly responsive to molecular binding events, such as the attachment of bacterial cells to a sensor surface[9]. The ability

Department of Electrical and Computer Engineering, University of Mohaghegh Ardabili, Ardabil, Iran. ✉email: heidarzadeh@uma.ac.ir

of plasmonic biosensors to detect minute changes in their environment has positioned them as promising tools for applications ranging from clinical diagnostics to environmental surveillance[10]. Also, in recently, there has been a significant increase in research focused on plasmonic devices due to their unique ability to manipulate light at the nanoscale. A wide range of applications have been explored in this field, including inverse photonic structures[11], nanoantennas[12], optical demultiplexers[13], interferometric systems[14], optical couplers[15], logic gates for computing purposes[16], and various types of highly sensitive sensors[17]. These studies aim to harness the extraordinary optical properties of surface plasmons to develop compact, high-speed, and energy-efficient photonic components for next-generation technologies.

Within the domain of plasmonic biosensing, metal-insulator-metal (MIM) waveguide structures have emerged as a particularly promising platform[18]. These structures consist of a dielectric layer sandwiched between two metallic layers, forming a nanoscale gap that supports plasmonic gap modes with intense field confinement[19]. The strong localization of the electric field within this gap enhances the interaction between light and the analyte, resulting in heightened sensitivity compared to other plasmonic configurations, such as single metal-dielectric interfaces[20]. Additionally, MIM waveguides strike a balance between field confinement and propagation losses, making them well-suited for practical biosensing applications[21]. Their planar geometry further facilitates integration with microfluidic systems and on-chip electronic components, paving the way for compact, high-throughput diagnostic devices[22].

The incorporation of ring resonator geometries into MIM waveguides has further advanced their utility in biosensing[23]. Ring resonators exhibit sharp resonance peaks in their transmission or reflection spectra, which shift in response to changes in the surrounding refractive index caused by analyte binding[24]. This shift, often quantified as a change in resonance wavelength ($\Delta\lambda$), serves as the basis for label-free detection, enabling real-time monitoring and quantitative analysis of bacterial concentrations[25]. The high sensitivity of these resonances, combined with their FOM, makes MIM ring resonators particularly effective for detecting biological entities, including pathogenic bacteria such as Escherichia coli, Staphylococcus aureus, and Vibrio cholerae[26]. Advances in nanofabrication techniques, such as electron beam lithography and nanoimprint lithography, have enabled the precise construction of these structures, further improving their performance and reproducibility[27].

Despite these advancements, several challenges persist in the development of MIM-based plasmonic biosensors for bacterial detection. One major limitation is their specificity in complex biological matrices, where non-target molecules can interfere with sensor responses, reducing accuracy[28]. Additionally, achieving a high signal-to-noise ratio remains difficult, particularly in low-concentration samples, due to intrinsic plasmonic losses in metals and manufacturing imperfections[29]. Surface functionalization, which is critical for selectively binding target bacteria, also poses a challenge, as robust and reproducible strategies are still under development[30]. Furthermore, while previous studies have demonstrated the feasibility of MIM biosensors for bacterial detection, many have focused on single-parameter optimization (e.g., sensitivity) without addressing the trade-offs between sensitivity, FOM, and limit of detection[31]. This has left a gap in the literature regarding comprehensive designs that simultaneously optimize multiple performance metrics and demonstrate practical applicability in real-world scenarios.

The present study addresses these research gaps by proposing a plasmonic optical biosensor based on a dual MIM ring resonator system for various bacterial detection. This work systematically optimizes the geometric parameters of the MIM structure to achieve a balance between sensitivity and FOM, leveraging 3D finite difference time domain (FDTD) simulations to model resonance behavior under bacterial binding conditions. By evaluating key performance metrics—sensitivity, figure of merit (FOM), and limit of detection (LoD) this study provides a detailed analysis of the sensor's capabilities. Moreover, the design demonstrates the ability to discriminate between different bacterial species based on their unique refractive index profiles, a feature that enhances its specificity and clinical relevance. Unlike prior works that often prioritized theoretical performance over practical integration, this research emphasizes the potential for on-chip implementation, offering a pathway toward high-throughput, label-free diagnostic platforms. By bridging the gap between sensitivity optimization and real-world applicability, this study contributes to the advancement of plasmonic biosensors as viable tools for revolutionizing bacterial detection in clinical and industrial settings.

Structure and method

The emergence of metamaterials has facilitated the development of metal-insulator-metal (MIM) nanoring structures[32]. These structures, which consist of subwavelength metallic elements, demonstrate a notably strong electromagnetic response. Metamaterials are characterized by exceptional properties such as electrical conductivity and negative magnetic permeability, making them ideal for constructing MIM nanoring structures. Among various metamaterials, gold, silver, and aluminum are considered the most important materials for building these structures[33]. In this study, gold, silver, and aluminum are used as metamaterials to create a plasmonic multifunctional optical biosensor based on MIM nanorings. The insulating dielectric substrate is made of a layer of SiO_2. Additionally, to enhance the performance of the structure, three different back reflectors are incorporated, one made of gold and the other made of silver and aluminum. The optical properties of gold, silver, aluminum, and SiO_2 are derived from the data provided by Palick[34]. The refraction coefficients of the bacteria measured in this study were also extracted from[35]. MIM nanoring technology in optical sensors provides a simple and efficient design. These sensors outperform other plasmonic sensors, increasing research and exploration in this area. This section discusses the structure of the plasmonic multifunctional optical biosensor, which is based on MIM nanorings, along with its dimensional parameters. The design typically features one or more metal rings, which can take various geometric forms, such as squares or circles, with gold being the preferred material for the nanorings. When these nanorings are exposed to a time-varying magnetic field, an annular electric current is induced, generating a magnetic dipole moment perpendicular to the nanoring. Figure 1 illustrates the

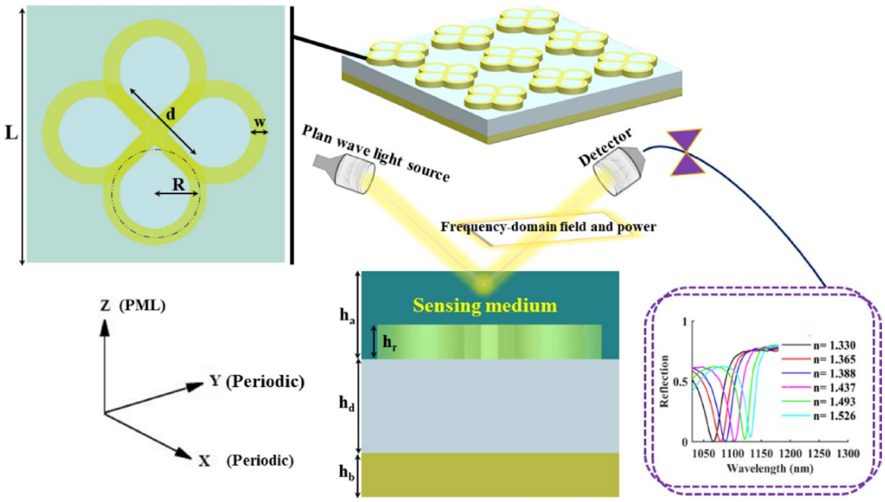

Fig. 1. Schematic of the designed MIM structure as a plasmonic biosensor(LibreOffice version 25.2.3 (URL: https://www.libreoffice.org/download/download-libreoffice/) and GIMP version 3.0.4 (URL: https://www.gimp.org/)).

Parameter	Symbol	Value
Dielectric length	L	780 nm
Arms length	d	310 nm
Width of rings	w	50 nm
The radius of the ring	R	130 nm
Back Reflector thickness	h_b	100 nm
Dielectric thickness	h_d	205 nm
Rings and arms thickness	h_r	75 nm
Analyte thickness	h_a	200 nm

Table 1. Dimensional parameters of the sensor after optimization.

design of the structure, which includes two nanorings and two perpendicular arms. This specific arrangement aims to maximize the sensor's performance.

Eight-shaped gold nanorings with radius R are arranged perpendicularly on a glass substrate in a side-by-side configuration. The width of the rings and arms is designated as W_r, while the arms' length is represented as d, and the thickness of both the nanorings and arms is denoted as h_r. Additionally, the structure incorporates a dielectric layer as the substrate for the nanorings, with side length L and thickness h_d. To further enhance the sensor's performance, a back reflector layer is added beneath the dielectric layer, with a thickness of h_b. Thus, the materials and dimensional parameters of the structure are analyzed to optimize the sensor's performance. Table 1 presents the dimensional characteristics of the structure after optimization. The impact of plasmonic losses and defects caused by manufacturing tolerances can significantly affect the performance of plasmonic systems. Metals used as plasmonic materials experience intrinsic energy losses primarily due to ohmic heating, which limits the strength of the local electric fields generated, thus affecting their use in biosensing applications. The level of loss depends on the chosen material. Manufacturing defects also introduce challenges, as imperfections in production can increase scattering losses, reducing the efficiency of these systems. For instance, surface roughness in metals can exacerbate scattering during transitions, leading to greater losses. Moreover, defects can disrupt the precise alignment and dimensions of plasmonic structures, causing discrepancies between experimental results and theoretical predictions. By carefully evaluating geometric dimensions, selecting suitable materials, and improving manufacturing processes, the efficiency and utility of plasmonic devices can be enhanced, opening up new opportunities for their application in various technological fields[29].

Developing MIM nanoring configurations, which are versatile systems for detecting various medical samples, including viruses, in laboratory environments, begins with their design and fabrication. To construct these structures, several nanofabrication techniques are employed, such as electron beam nanolithography (EBL), focused ion beam lithography (FBL), and nanoimprint lithography[27]. Furthermore, MIM nanoring structures are integrated with microfluidic systems to investigate the permeability characteristics of liquid medical samples. The interaction of biological samples with the MIM nanoring structure alters the optical properties of the sensing environment, causing a shift in the resonance frequency that can be measured and analyzed[23].

The proposed system is analyzed using the finite difference time domain (FDTD) numerical method, where Maxwell's equations are solved through the Yee algorithm. For this purpose, the commercially available Lumerical

FDTD analyzer, widely used in optics, photonics, and nanoelectronics, is employed. In the FDTD method, the mesh is set as auto-non-uniform, with the Conformal 0 mode applied to modify it. Indeed, it is well recognized that in Lumerical FDTD Solutions, the Conformal variant 1 mesh refinement is typically preferred for metallic materials due to its enhanced handling of sharp field gradients and high refractive index contrasts. Conversely, Conformal variant 0 is generally associated with dielectric regions. However, it is important to note that the choice between these variants is not always strictly binary. In certain cases, particularly at metal–dielectric interfaces, Conformal 0 can also be effectively applied, depending on the structural configuration and the nature of the simulation goals. Mesh accuracy is set to 10 nm, and a separate mesh with dx = dy = dz = 2 nm is used in the structure-sensitive regions of the MIM nanorings. The refractive index of the background is set to that of air, which is 1. The simulation time is fixed at 1000 fs with a temperature of 300 K, utilizing the Field Time monitor. Perfectly matched layer (PML) boundary conditions are applied along the z-axis, while periodic boundary conditions are used in the x and y directions. Light is sourced from a flat wave, with wavelengths ranging from 1000 to 1300 nm. The reflection spectrum is analyzed using the Frequency-domain field and power monitor, and the distribution of the electromagnetic field is visualized with the Frequency-domain field profile monitor. To assess sensor performance, including sensitivity and figure of merit (FOM), an analyte layer can be placed on the MIM nanoring structure. Adjusting the refractive index of the analyte (Δn_s) results in a shift in the reflection spectrum at the resonance wavelength ($\Delta\lambda_0$). The sensor's sensitivity is mathematically defined as[24]:

$$\mathrm{S} = \frac{\Delta\lambda_0}{\Delta \mathrm{n_s}} \tag{1}$$

The FOM is a quantitative metric used to evaluate and compare the overall performance of an optical sensor. It consolidates multiple performance parameters, such as sensitivity and response time, into a single value that simplifies comparative analysis among sensors or technologies. The sensor's FOM can be mathematically expressed as follows[25]:

$$\mathrm{FOM} = \frac{\mathrm{S}}{\mathrm{FWHM}} \tag{2}$$

Here, FWHM represents the full width at half maximum, an essential parameter in optical sensor technology. FWHM characterizes the quality of the resonances in the reflection spectrum and provides valuable insight into the sensor's overall quality and sensitivity. A smaller FWHM is preferred as it indicates better resolution in detecting the resonance of biological samples.

Additionally, the lowest measurable value that the sensor can detect is known as the Limit of Detection (LoD), defined as[30]:

$$\mathrm{LoD} = \left(\frac{\Delta\ \mathrm{n_s}}{1.5}\right) \times \left(\frac{\mathrm{FWHM}}{\Delta\ \lambda_0}\right)^{1.25} \tag{3}$$

Results and discussion

Optimizing the structural parameters of the metal-insulator-metal (MIM) nanoring biosensor is crucial for enhancing its performance in rapid bacterial detection. Figure 2(a), (b), and (c) presents the reflectance spectra of the MIM structure, simulated using 3D FDTD methods over a 1000–1300 nm wavelength range, to assess the effects of varying the thicknesses of the back reflector (h_b), dielectric layer (h_d), and nanorings (h_r). Reflectance is normalized between 0 and 1, with baseline parameters (ring radius $R = 130$ nm, ring width W_r = 50 nm) and material configuration (gold nanorings, gold back reflector, SiO_2 dielectric) set per Table 1. Figure 2(a) examines the reflectance spectra for back reflector thicknesses (h_b) from 94 nm (black dashed curve) to 104 nm (yellow dashed curve). Decreasing h_b to 94 nm shifts the resonance to 1115 nm with a minimum reflectance of 0.04, while increasing h_b to 104 nm shifts it to 1125 nm with a minimum reflectance of 0.06 and an FWHM of 38 nm, indicating higher scattering losses. Figure 2(b) analyzes the spectra for dielectric layer thicknesses (h_d) from 205 nm (black dashed curve) to 215 nm (yellow dashed curve). At the h_d = 205 nm, the resonance occurs at 1120 nm with a minimum reflectance of 0.05 and an FWHM of 31.88 nm. Increasing the h_d to 207 nm and 209 nm shifts the resonance to 1122 nm and 1124 nm, respectively, with a minimum reflectance of 0.06, while h_d = 215 nm results in a resonance at 1128 nm with a minimum reflectance of 0.07, reflecting reduced field confinement. Figure 2(c) evaluates the spectra for nanoring thicknesses (h_r) from 65 nm (black dashed curve) to 75 nm (yellow dashed curve). At the h_r = 75 nm, the resonance is at 1120 nm with a minimum reflectance of 0.05. Decreasing h_r to 65 nm shifts the resonance to 1110 nm with a minimum reflectance of 0.03, while increasing h_r to 73 nm shifts it to 1122 nm with a minimum reflectance of 0.06, indicating higher plasmonic losses. The h_r = 75 nm balances field enhancement and loss minimization. The Fig. 2(d) examines the reflectance spectra for h_a values from 185 nm (black dashed curve) to 210 nm (yellow dashed curve). When h_a is 185 nm, the resonance dip is observed at approximately 1120 nm with a minimum reflectance of about 0.03. As h_a increases, there is a clear trend, The resonance wavelength progressively shifts. For instance, increasing h_a to 190 nm shifts the resonance to around 1125 nm, and this shift continues as h_a is further increased to 195 nm (approx. 1130 nm), 200 nm (approx. 1135 nm), 205 nm (approx. 1140 nm), and finally to 210 nm, where the resonance occurs at the longest wavelength in this set, around 1145 nm. Throughout these variations in h_a, the minimum reflectance, indicating the strength of the resonance, remains relatively low and consistent, generally below 0.05. Thus, the primary effect of increasing h_a from 185 nm to 210 nm is a systematic shift of the resonance to longer wavelengths, while the depth of the reflectance dip remains largely unchanged.

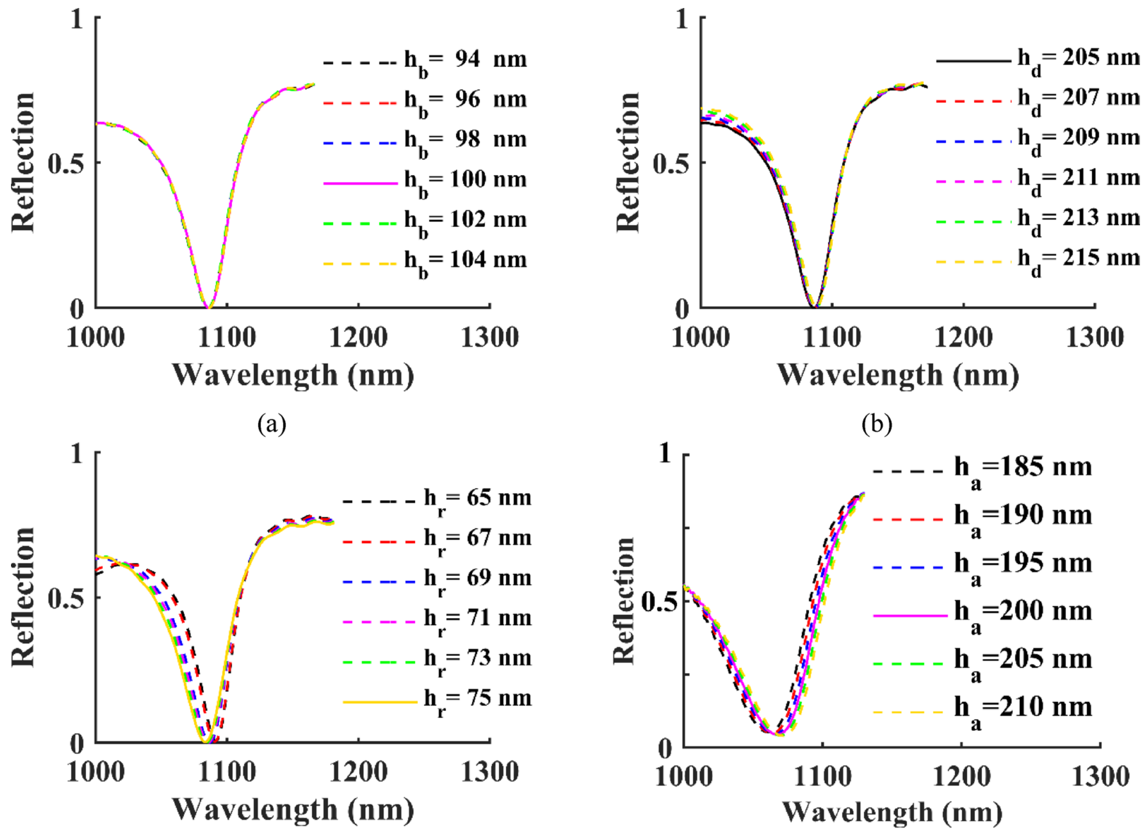

Fig. 2. PSO optimization results (**a**) reflectance spectra for different back reflector thicknesses, (**b**) reflectance spectra for different dielectric layer thicknesses, (**c**) reflectance spectra for different nanoring thicknesses, and (**d**) reflectance spectra for different sensing medium thicknesses.

Figure 3 illustrates the optimization results obtained using Particle Swarm Optimization (PSO), showing how variations in structural parameters affect the sensitivity and figure of merit of the proposed metal-insulator-metal (MIM) plasmonic biosensor. Each subfigure (a–d) presents the response of sensitivity (blue line, left y-axis) and FOM (red line, right y-axis) to changes in a specific design parameter. In Fig. 3a, the thickness of the back reflector (h_b) is varied between 98 and 104 nm. Sensitivity peaks near 330 nm/RIU, while FOM reaches approximately 11 RIU^{-1} at an optimal point. The results highlight a trade-off between enhanced field confinement and increased plasmonic losses. Figure 3b analyzes the effect of dielectric layer thickness (h_d) ranging from 205 to 215 nm. Both sensitivity and FOM decrease as h_d increases, indicating that thicker dielectric layers weaken the electromagnetic field confinement and reduce the interaction between the guided mode and the sensing medium. In Fig. 3c, the thickness of the nanorings (h_r) is varied from 65 to 75 nm. Sensitivity shows an overall increasing trend, with a maximum of about 330 nm/RIU at h_r = 75 nm. The FOM also follows a slightly oscillating pattern, peaking near 10.5 RIU^{-1}. This suggests that a properly tuned nanoring thickness can minimize ohmic losses and enhance resonance sharpness. Figure 3d investigates the analyte layer thickness (h_a) from 185 to 210 nm. Increasing h_a causes a moderate shift in sensitivity and FOM, with optimal performance occurring around 200–205 nm. This behavior reflects the importance of maximizing field overlap between the sensing layer and the confined plasmonic modes. Overall, these optimization results confirm that the biosensor's performance is highly dependent on the precise tuning of multiple parameters. The PSO algorithm effectively identifies configurations that achieve a balance between sensitivity and spectral resolution. The study underscores the necessity of multi-variable optimization in plasmonic sensor design to achieve reliable, high-performance detection suitable for real-world biomedical applications.

The choice of materials for the back reflector and nanorings significantly impacts the performance of the metal-insulator-metal (MIM) nanoring biosensor, particularly its resonance characteristics and sensitivity for bacterial detection. Figure 4(a) and (b) present the reflectance spectra of the MIM structure, simulated via 3D FDTD in the 1000–1300 nm range, to evaluate gold (Au), silver (Ag), and aluminum (Al). Optimized parameters from Table 1 (ring radius $R = 130$ nm, dielectric thickness h_d = 205 nm, back reflector thickness h_b = 100 nm, nanoring thickness h_r = 75 nm) and baseline conditions (TE polarization, 300 K, normal incidence $\theta = 0°$) were applied. Figure 4(a) compares the reflectance spectra for back reflectors of gold, silver, and aluminum (with gold nanorings). The gold back reflector exhibits a resonance dip at 1120 nm with a minimum reflectance of 0.05 and an FWHM of 31.88 nm (as per Table 2). A silver back reflector shifts the resonance to 1118 nm with a minimum reflectance of 0.04, but its chemical instability in biological environments limits its use. An aluminum

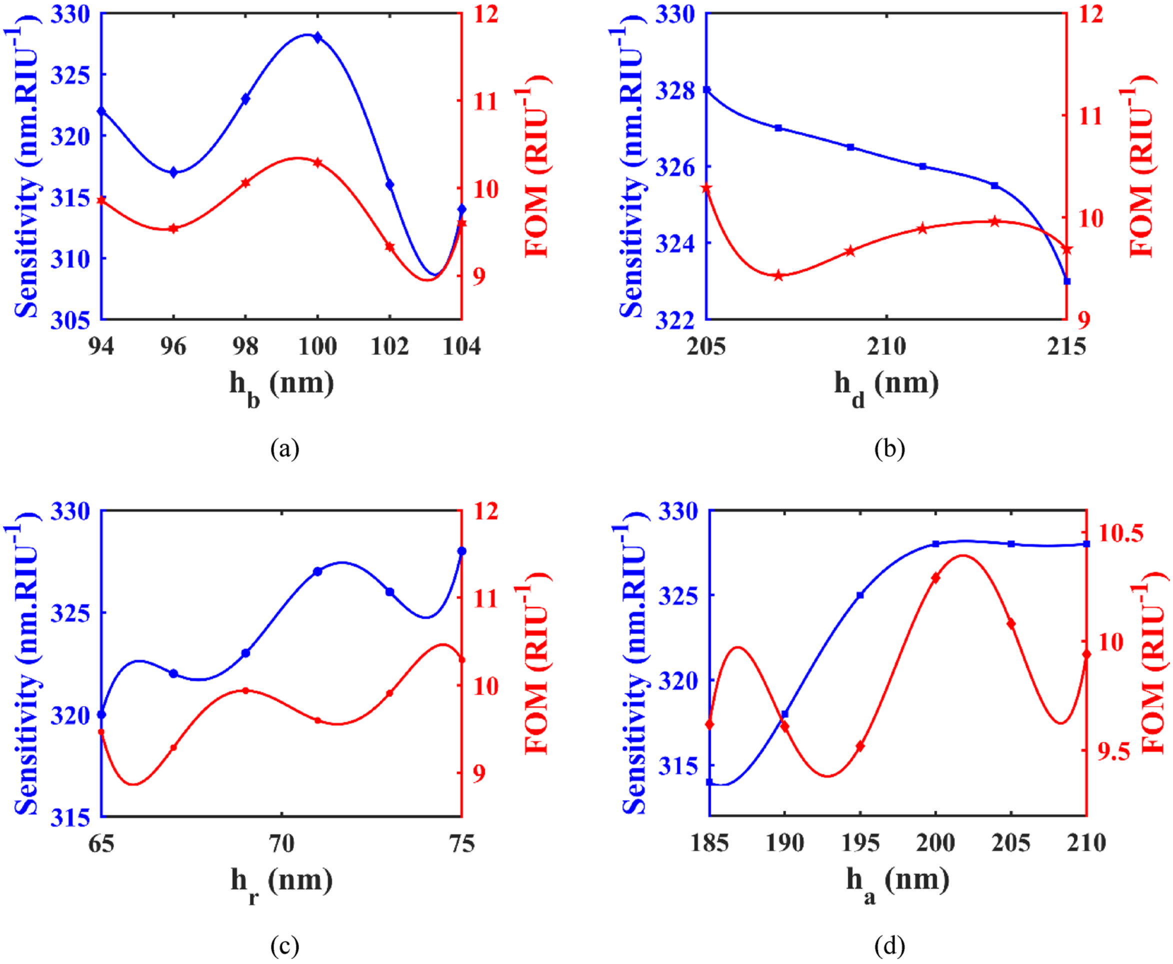

Fig. 3. PSO optimization results. (**a**) Sensitivity and FOM for different back reflector thicknesses, (**b**) sensitivity and FOM for different dielectric layer thicknesses, (**c**) sensitivity and FOM for different nanoring thicknesses, and (**d**) Sensitivity and FOM for different sensing medium thicknesses.

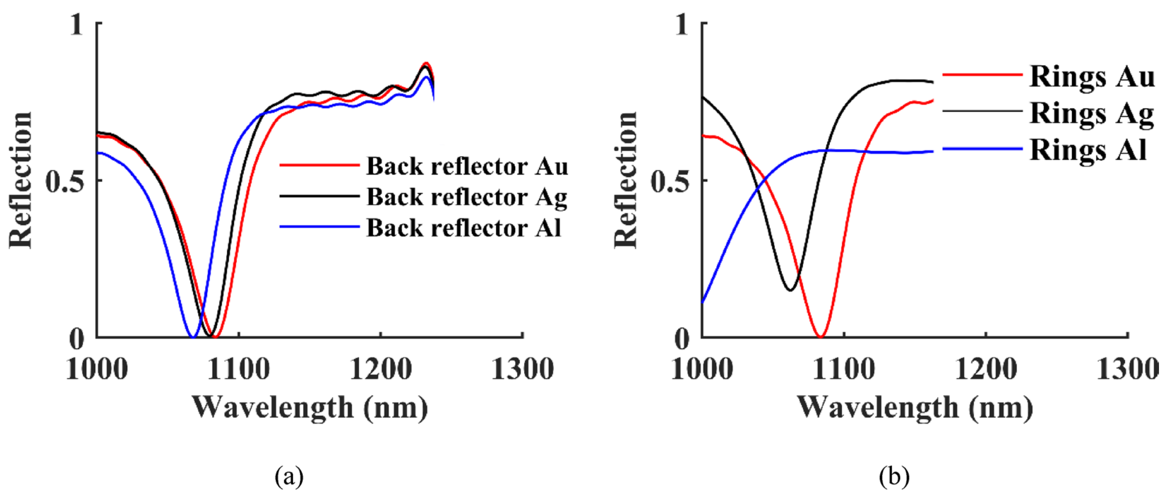

Fig. 4. (**a**) Reflectance spectra with different back reflector materials and (**b**) reflectance spectra with different nanoring materials.

References	Sensitivity (nm.RIU^{-1})	FWHM (nm)	FOM (RIU^{-1})	LoD
[30]	66	0.9	7.7	---
[27]	150	20	7.5	0.1
[24]	200	25	8	0.09
[37]	225	---	---	---
[25]	280	35	8	0.08
[38]	300	---	---	---
[31]	313	39.1	4	---
This work	324.76	31.88	10.187	0.075

Table 2. Comparison of performance parameters of four resonance modes of the proposed structure with previously reported works.

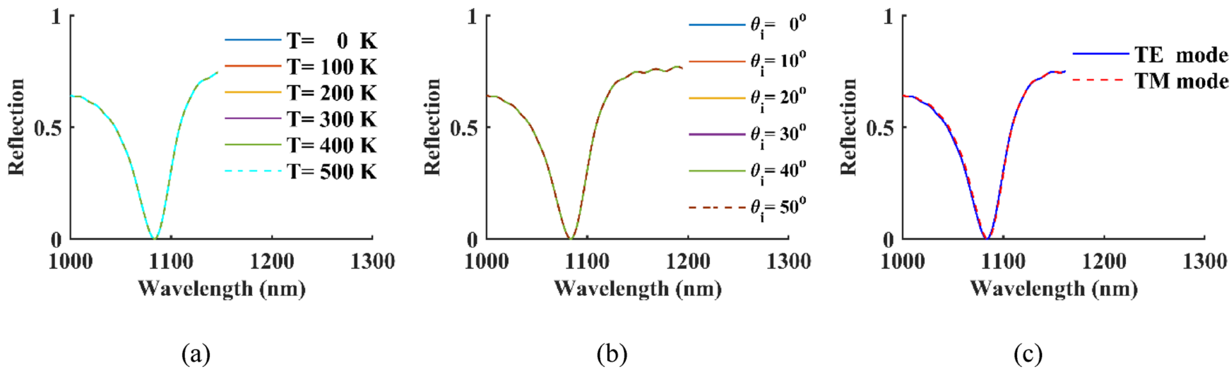

Fig. 5. (**a**) Reflectance spectra at different temperatures, (**b**) reflectance spectra at different incident angles and (**c**) reflectance spectra for TE and TM polarization modes.

back reflector results in a resonance at 1125 nm with a minimum reflectance of 0.08, indicating higher losses. Gold was selected for its optimal balance of optical performance and chemical stability. Figure 4(b) examines the spectra for nanorings of gold, silver, and aluminum (with a gold back reflector). Gold nanorings show a resonance at 1120 nm with a minimum reflectance of 0.05. Silver nanorings shift the resonance to 1117 nm with a minimum reflectance of 0.03, but their chemical instability poses challenges. Aluminum nanorings result in a resonance at 1128 nm with a minimum reflectance of 0.09, reflecting greater plasmonic losses. The combination of a gold back reflector and gold nanorings maximizes sensitivity and resolution while ensuring stability in biological settings.

The robustness of the metal-insulator-metal (MIM) nanoring biosensor under varying environmental and operational conditions is essential for its practical application in bacterial detection. Figure 5 (a), (b), and (c) presents the reflectance spectra of the optimized MIM structure, simulated using 3D finite difference time domain (FDTD) methods with the Lumerical FDTD aThe robustness of the metal-insulator-metal (MIM) nanoring biosensor across a range of environmental and operational conditions is a critical factor for its practical use in bacterial detection. Figure 5 (a), (b), and (c) illustrates the reflectance spectra of the optimized MIM structure, simulated using 3D finite-difference time-domain (FDTD) methods with the Lumerical FDTD analyzer. These simulations were performed over a wavelength range of 1000 to 1300 nm, with the reflectance normalized between 0 and 1. The optimized parameters from Table 1 (e.g., ring radius $R = 130$ nm, dielectric thickness h_d = 205 nm, back reflector thickness h_b = 100 nm, nanoring thickness h_r = 75 nm) and the material configuration (gold nanorings, gold back reflector, SiO_2 dielectric) were applied. As observed in Figs. 5 (a), (b), and (c), the reflectance spectra of the MIM nanoring structure exhibit remarkable consistency despite variations in temperature, incident angle, and polarization mode. Notably, the spectra overlap significantly across all tested conditions, indicating minimal sensitivity to these external factors. This stability and relative insensitivity to environmental and operational changes highlight a key strength of the MIM nanoring biosensor, making it well-suited for real-world applications where conditions may not always be ideal. For instance, in practical settings, the temperature, angle of incoming light, or polarization of the light source may vary, yet the sensor's performance remains reliable. The findings demonstrate that the sensor exhibits polarization independence, maintaining consistent performance regardless of the incident light's polarization orientation. This behavior can be attributed to its symmetric structural design and the incorporation of nanostructures that enable uniform light absorption across all polarization states. Such polarization-insensitive operation enhances the sensor's suitability for real-world applications, as it removes the requirement for polarization alignment in varying environmental conditions. Consequently, the MIM nanoring biosensor emerges as a robust and dependable tool for bacterial detection, capable of delivering consistent performance even under diverse and non-ideal conditions, which is a crucial attribute for its deployment in practical biosensing applications.

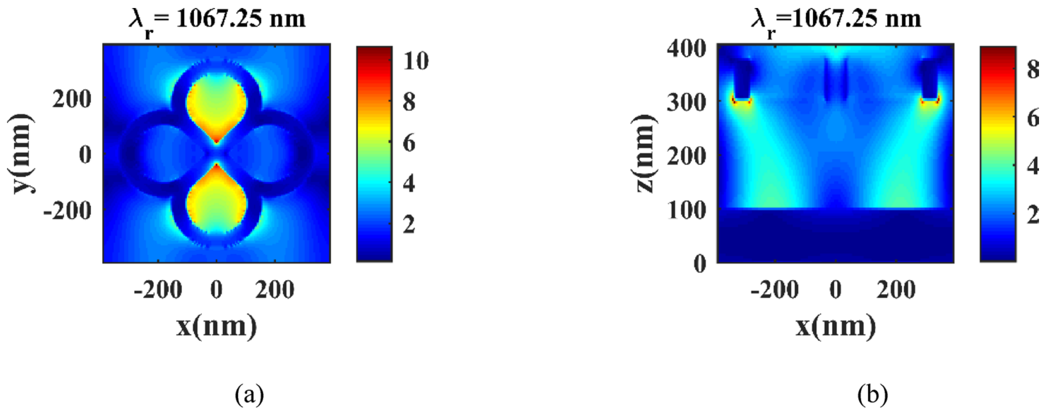

Fig. 6. (**a**) Electric field distribution in the XY-plane and (**b**) electric field distribution in the XZ-plane.

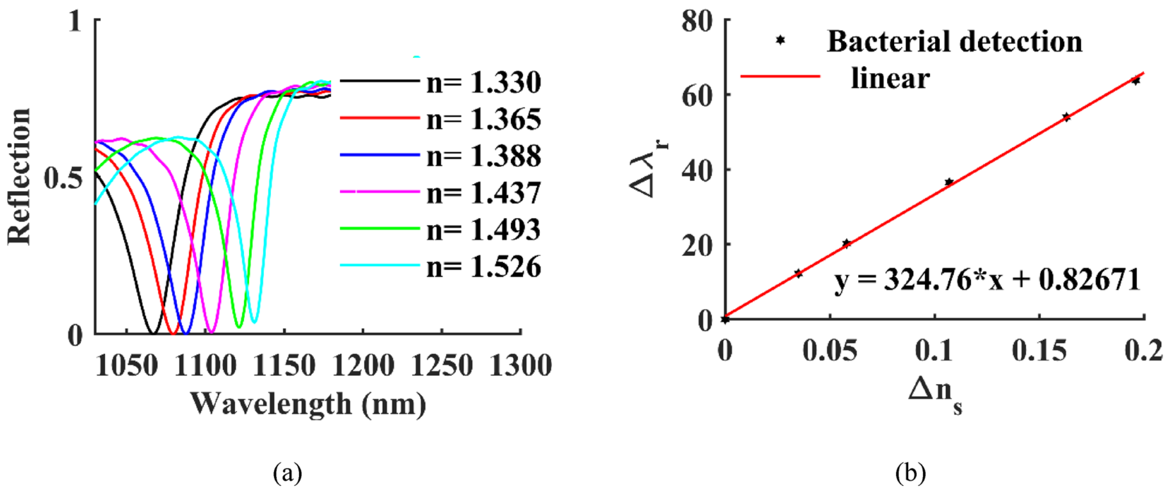

Fig. 7. (**a**) Reflectance spectra of the structure and detection of Vibrio cholera bacteria at $n = 1.365$ (red curve), E. coli bacteria at $n = 1.388$ (blue curve), Pseudomonas bacteria at $n = 1.437$, 1.493 and 1.526 (violet-green and turquoise curves) and (**b**) changes in resonance wavelength versus changes in the refractive index of the sensor's sensing medium in the presence of different bacteria as a curve fit.

The electric field distribution in the metal-insulator-metal (MIM) nanoring structure is crucial for its sensitivity to bacterial detection. Figure 6 (a) and (b) shows the field intensity at 1067.25 nm, simulated via 3D FDTD, using optimized parameters ($R = 130$ nm, h_d = 205 nm) and materials (gold nanorings, gold back reflector). Figure 6(a) displays the field intensity in the XY-plane (z = 0 nm), with x and y axes from − 390 nm to 390 nm. The color bar (0–10) shows a quadrupole-like pattern, with a maximum intensity of 10 around the nanorings, indicating strong SPP excitation at the gold-dielectric interface. This enhancement boosts the sensor's sensitivity to analyte refractive index changes. Figure 6(b) shows the field in the XZ-plane (y = 0 nm), with x from − 390 nm to 390 nm and z from 0 to 400 nm. The color bar (0–8) reveals field confinement in the dielectric gap (z ≈ 75–280 nm), peaking at 8 near the nanorings (z ≈ 75 nm). The field extends into the analyte layer (z > 280 nm), decaying exponentially, which enhances interaction with bacterial analytes.

The strong field confinement supports the sensor's high sensitivity (324.76 nm.RIU^{-1}) and FOM (10.187 RIU^{-1}), as per Table 2, enabling effective bacterial detection.

The metal-insulator-metal (MIM) nanoring biosensor's ability to detect bacteria is evaluated in Figs. 7 (a) and (b) using FDTD simulations (wavelength 1000–1300 nm) with the optimized structure (gold back reflector and nanorings). Figure 7(a) shows reflectance spectra for a reference medium ($n = 1.330$, black curve), Vibrio cholerae bacterial ($n = 1.365$, red curve), E. coli bacterial ($n = 1.388$, blue curve), and Pseudomonas species ($n = 1.437$, 1.493, 1.526; violet, green, turquoise curves). The resonance shifts from 1115 nm (reference) to 1120 nm (Vibrio cholerae), 1125 nm (E. coli), and up to 1140 nm (Pseudomonas at $n = 1.526$), with the FWHM increasing slightly to 38 nm at $n = 1.526$. This red-shift reflects the sensor's sensitivity to refractive index changes.

Figure 7(b) plots the resonance wavelength shift (Δλ) versus refractive index change (Δn), with data points for the bacteria ($\Delta n = 0.035$ to 0.196). A linear fit (y = 324.76x + 0.82671) yields a sensitivity of 324.76 nm.RIU^{-1}, matching Table 2. This linearity enables quantitative bacterial differentiation, outperforming prior sensors.

Nanostructures are particularly suitable for the miniaturization of optical circuits due to their compact dimensions and compatibility with existing nanofabrication technologies. The choice of the MIM (Metal–Insulator–Metal) structure aligns with current trends in plasmonic sensor development, aimed at enhancing sensitivity, tunability, and integration capabilities for advanced biosensing and chemical detection. The integration of MIM structures allows for a straightforward yet efficient design, encouraging further investigation into their potential applications. To create these structures, state-of-the-art fabrication methods such as electron beam lithography (EBL), focused ion beam lithography (FBL), and nanoimprint lithography are employed[29]. Additionally, microfluidic systems have been incorporated to analyze liquid medical samples, where variations in resonant frequency caused by sample interactions are used to detect property changes[36]. For successful manufacturing, design optimization must consider real-world fabrication limitations, including minimum feature sizes and alignment tolerances, to avoid impractical or overly complex structures. EBL, a widely used nanofabrication method, can consistently produce features as small as ~10 nm, though going smaller becomes increasingly challenging due to process limitations. By incorporating these constraints into the design optimization process, the resulting devices perform well and are feasible to fabricate using existing technologies.

A comprehensive evaluation of the proposed metal-insulator-metal (MIM) nanoring biosensor's performance is essential to establish its superiority over existing plasmonic biosensors for rapid bacterial detection. Table 2 presents a detailed comparison of the key performance metrics sensitivity, full width at half maximum (FWHM), figure of merit (FOM), and limit of detection (LoD) of the proposed structure against several previously reported works. These metrics were obtained through 3D finite difference time domain (FDTD) simulations using the optimized parameters. The comparison highlights the proposed sensor's advancements in sensitivity, resolution, and detection capability, addressing the research gap of achieving high specificity and sensitivity in complex biological matrices. The proposed MIM nanoring biosensor achieves a sensitivity of 324.76 nm.RIU^{-1}, an FWHM of 31.88 nm, an FOM of 10.187 RIU^{-1}, and a LoD of 0.075, as reported in Table 2. The high sensitivity reflects the sensor's ability to detect small refractive index changes induced by bacterial binding, as demonstrated by resonance shifts of 5–25 nm for Vibrio cholerae bacterial ($n = 1.365$), E. coli bacterial ($n = 1.388$), and Pseudomonas species ($n = 1.437–1.526$) (Fig. 6). The narrow FWHM of 31.88 nm indicates a sharp resonance profile, which enhances the sensor's resolution and ability to distinguish closely spaced refractive index changes, a critical feature for differentiating bacterial species.

Comparing these results with prior works, Reference[33] reports a sensitivity of 66 nm.RIU^{-1}, an FWHM of 0.9 nm, an FOM of 7.7 RIU^{-1}. While the extremely narrow FWHM suggests high resolution, the low sensitivity severely limits its ability to detect small refractive index changes, making it less suitable for bacterial detection in complex biological samples. Reference[29] achieves a sensitivity of 150 nm.RIU^{-1}, an FWHM of 20 nm, an FOM of 7.5 RIU^{-1}, and a LoD of 0.1, reflecting moderate performance but still falling short of the proposed sensor's sensitivity and FOM. Reference[31] reports a sensitivity of 200 nm.RIU^{-1}, an FWHM of 25 nm, an FOM of 8 RIU^{-1}, and a LoD of 0.09, showing improved sensitivity over Reference[29] but with a broader FWHM and lower FOM compared to this work. Reference[35] achieves a sensitivity of 225 nm.RIU^{-1} but lacks data on FWHM, FOM, and LoD, making it difficult to fully assess its performance; however, its sensitivity is notably lower than the proposed sensors. Reference[32] reports a sensitivity of 280 nm.RIU^{-1}, an FWHM of 35 nm, an FOM of 8 RIU^{-1}, and a LoD of 0.08, which is closer to the proposed sensor's performance but still lags in sensitivity, FOM, and LoD. Reference[29] achieves a sensitivity of 300 nm.RIU^{-1}, again without FWHM, FOM, or LoD data, indicated a higher sensitivity than Reference[35] but still below the proposed sensor's performance. Finally, Reference[34] reports a sensitivity of 313 nm.RIU^{-1}, an FWHM of 39.1 nm, an FOM of 4 RIU^{-1}, and no LoD specified. Although its sensitivity is the closest to the proposed sensor among the references, the broader FWHM and significantly lower FOM indicate reduced resolution and overall performance.

Conclusion

This study successfully developed and evaluated a plasmonic optical biosensor based on a metal-insulator-metal (MIM) dual-ring resonator structure, demonstrating its potential as a highly effective platform for rapid, label-free bacterial detection. Through rigorous optimization using the Particle Swarm Optimization (PSO) algorithm and 3D finite-difference time-domain (FDTD) simulations, the sensor achieved an impressive sensitivity of 324.76 nm·RIU^{-1}, a figure of merit (FOM) of 10.187 RIU^{-1}, and a limit of detection (LoD) of 0.075. These performance metrics enabled the sensor to effectively detect and differentiate bacterial species, including *Vibrio cholerae* ($n = 1.365$), *Escherichia coli* ($n = 1.388$), and *Pseudomonas* species ($n = 1.437–1.526$), with resonance wavelength shifts ranging from 5 to 25 nm. This capability underscores the sensor's ability to quantitatively distinguish bacteria based on their refractive index profiles, addressing a critical research gap in the specificity and sensitivity of plasmonic biosensors within complex biological matrices. The sensor's robust performance under varying environmental conditions—such as temperature (0–500 K), incident angle (0°–50°), and polarization modes (TE and TM)—further highlights its practical applicability in real-world settings. Additionally, the planar geometry of the MIM structure facilitates its integration into test-on-a-chip platforms, paving the way for high-throughput bacterial detection in clinical diagnostics, food safety, and environmental monitoring. Future research should focus on experimental validation using real biological samples, improving surface functionalization strategies to enhance specificity, and exploring scalability for commercial deployment. By bridging the gap between theoretical optimization and practical implementation, this work positions the MIM nanoring biosensor as a promising tool for advancing rapid and reliable bacterial detection.

Data availability

The datasets used and/or analyzed during the current study are available from the corresponding author upon reasonable request.

Received: 15 April 2025; Accepted: 13 June 2025
Published online: 01 July 2025

References

1. Escobar, V. et al. Recent advances on peptide-based biosensors and electronic noses for foodborne pathogen detection. *Biosensors* **13**(2), 258 (2023).
2. Franco-Duarte, R. et al. Advances in chemical and biological methods to identify microorganisms—from past to present. *Microorganisms* **7**(5), 130 (2019).
3. Bravo-Frank, N. et al. Realtime bacteria detection and analysis in sterile liquid products using deep learning holographic imaging. *Npj Biosensing*. **1**(1), 8 (2024).
4. Shahbaz, M., Butt, M. A. & Piramidowicz, R. A concise review of the progress in photonic sensing devices. In *Photonics*, MDPI, 698. Accessed 03 Apr 2025 https://www.mdpi.com/2304-6732/10/6/698 (2023).
5. Hamza, M. E., Othman, M. A. & Swillam, M. A. Plasmonic biosensors. *Biology* **11**(5), 621 (2022).
6. Maier, S. A. & Atwater, H. A. Plasmonics: localization and guiding of electromagnetic energy in metal/dielectric structures. *J. Appl. Phys.* **98**(1), (2005).
7. Butt, M. A. Loop-terminated Mach–Zehnder interferometer integrated with functional polymer for CO2 gas sensing. *Appl. Sci.* **14**(11), 4714 (2024).
8. Butt, M. A. Plasmonic sensors based on a metal–insulator–metal waveguide—what do we know so far? *Sensors* **24**(22), 7158 (2024).
9. Jain, M. C., Nadaraja, A. V., Narang, R. & Zarifi, M. H. Rapid and real-time monitoring of bacterial growth against antibiotics in solid growth medium using a contactless planar microwave resonator sensor. *Sci. Rep.* **11**(1), 14775 (2021).
10. Shahrajabian, M. H. & Sun, W. Various techniques for molecular and rapid detection of infectious andepidemic diseases. *LOC* **20**(9), 779–801. https://doi.org/10.2174/1570178620666230331095720 (2023).
11. Mahadi, M. K., Rahad, R., Haque, M. A. & Nishat, M. M. Gated recurrent unit (GRU)-based deep learning method for spectrum estimation and inverse modeling in plasmonic devices. *Appl. Phys. A*. **130**(11), 784 (2024).
12. Rahad, R., Mohsin, A. S., Bhuian, M. B. H. & Rahman, M. M. Graphene-metamaterial based tunable broadband polarization insensitive absorber for Terahertz antenna design. *Ieee Access.* **12**, 48654–48667 (2024).
13. Rahad, R. et al. A novel plasmonic MIM sensor using integrated 1\times 2 demultiplexer for individual lab-on-chip detection of human blood group and diabetes level in the visible to near-infrared region. *IEEE Sens. J.* (2024).
14. Butt, M. A., Shahbaz, M. & Piramidowicz, R. Racetrack ring resonator integrated with multimode interferometer structure based on low-cost silica–titania platform for refractive index sensing application. In *Photonics*, MDPI, 978 (Accessed 10 May 2025) https://www.mdpi.com/2304-6732/10/9/978 (2023).
15. Tian, J., Yu, S., Yan, W. & Qiu, M. Broadband high-efficiency surface-plasmon-polariton coupler with silicon-metal interface. *Appl. Phys. Lett.* **95**(1), (2009).
16. Haque, M. A., Rahad, R. & Faruque, M. O. Optical computing at the subwavelength scale: TeX\backslashbreak? A multifunctional MIM plasmonic logic gate. *Appl. Opt.* **63**(24), 6364–6370 (2024).
17. Rahad, R., Rakib, A. K. M., Haque, M. A., Sharar, S. S. & Sagor, R. H. Plasmonic refractive index sensing in the early diagnosis of diabetes, anemia, and cancer: an exploration of biological biomarkers. *Results Phys.* **49**, 106478 (2023).
18. Simoni, F., Khoo, I. & Umeton, C. *Novel Optical Materials*, vol. 1. Accessed 03 Apr 2025. https://books.google.com/books?hl=en&lr=&id=s_L3EAAAQBAJ&oi=fnd&pg=PR5&dq=+Li,+X.,+et+al.+(2023).+Balancing+confinement+and+loss+in+plasmonic+waveguides+for+biosensing.+Nanophotonics,+12(4),+567-578.&ots=m2ZezrhHdi&sig=iD4U5tW9_ONYmHZtbMF17HrNNtk (World Scientific, 2023).
19. Babicheva, V. E. Optical processes behind plasmonic applications. *Nanomaterials* **13**(7), 1270 (2023).
20. Huang, S. H. & Wu, P. C. Exploring plasmonic gradient metasurfaces for enhanced optical sensing in the visible spectrum. *Nanophotonics* **13**(7), 1099–1108. https://doi.org/10.1515/nanoph-2023-0809 (2024).
21. Valdiviezo, J. H. M. & Torchia, G. A. Design and development of integrated sensors under the silicon on insulator (SOI) platform for applications in the near/mid-infrared (NIR/MIR) band. In *Nanoengineering: Fabrication, Properties, Optics, Thin Films, and Devices XXI*, 77–90. Accessed 03 Apr 2025. https://www.spiedigitallibrary.org/conference-proceedings-of-spie/13116/131160D/Design-and-development-of-integrated-sensors-under-the-silicon-on/ https://doi.org/10.1117/12.3028216.short (SPIE, 2024).
22. Sharma, S., Kumar, R., Kumar, K. & Thakur, N. Sustainable applications of biowaste-derived carbon Dots in eco-friendly technological advancements: a review. *Mater. Sci. Engineering: B*. **305**, 117414 (2024).
23. Andam, N., Refki, S., Hayashi, S. & Sekkat, Z. Plasmonic mode coupling and thin film sensing in metal–insulator–metal structures. *Sci. Rep.* **11**(1), 15093 (2021).
24. Tang, Y., Zeng, X. & Liang, J. Surface plasmon resonance: an introduction to a surface spectroscopy technique. *J. Chem. Educ.* **87**(7), 742–746. https://doi.org/10.1021/ed100186y (2010).
25. Mostufa, S., Paul, A. K. & Chakrabarti, K. Detection of hemoglobin in blood and urine glucose level samples using a graphene-coated SPR based biosensor. *OSA Continuum*. **4**(8), 2164–2176 (2021).
26. Papadopoulos, C. *Nanofabrication*. In *SpringerBriefs in Materials*. https://doi.org/10.1007/978-3-319-31742-7 (Springer International Publishing, 2016).
27. Zhu, S., Tang, Y., Lin, C., Liu, X. Y. & Lin, Y. Recent advances in patterning natural polymers: from nanofabrication techniques to applications. *Small Methods*. **5**(3), 2001060. https://doi.org/10.1002/smtd.202001060 (2021).
28. Tokel, O., Inci, F. & Demirci, U. Advances in plasmonic technologies for point of care applications. *Chem. Rev.* **114**(11), 5728–5752. https://doi.org/10.1021/cr4000623 (2014).
29. Zhang, J. et al. Plasmonic metasurfaces with 42.3% transmission efficiency in the visible. *Light: Sci. Appl.* **8**(1), 53 (2019).
30. Alsalman, O. et al. Design of split ring resonator graphene metasurface sensor for efficient detection of brain tumor. *Plasmonics* **19**(1), 523–532. https://doi.org/10.1007/s11468-023-02002-9 (2024).
31. Taghipour, A. & Heidarzadeh, H. Design and analysis of highly sensitive LSPR-based metal–insulator–metal nano-discs as a biosensor for fast detection of SARS-CoV-2. In *Photonics*, MDPI, 542. Accessed 03 Apr 2025. https://www.mdpi.com/2304-6732/9/8/542 (2022).
32. Ren, Y., Duan, M., Guo, R. & Liu, J. Printed transformable liquid-metal metamaterials and their application in biomedical sensing. *Sensors* **21**(19), 6329 (2021).
33. Huang, Z., Droulias, S., Koschny, T. & Soukoulis, C. M. Mechanism of the metallic metamaterials coupled to the gain material. *Opt. Express*. **22**(23), 28596–28605 (2014).
34. Palik, E. D. *Handbook of optical constants of solids*, vol. 3. Accessed 03 Apr 2025. https://books.google.com/books?hl=en&lr=&id=nxoqxyoHfbIC&oi=fnd&pg=PP1&dq=Palik,+E.D.,+Handbook+of+optical+constants+of+solids.+Vol.+3.+1998:+Academic+press.&ots=EH-WMGy-de&sig=4eeTRwJzrMfQ8EJOnishP1wNd0E (Academic Press, 1998).
35. Khan, M. B., Hossain, B., Rahman, T., Ahmed, D. M. S. & Paul, A. K. Design and analysis of a highly sensitive BaTiO3—BP hybrid Structure-Based SPR biosensor for rapid bacterial detection. *Plasmonics* https://doi.org/10.1007/s11468-025-02798-8 (2025).
36. Mauriz, E. Recent progress in plasmonic biosensing schemes for virus detection. *Sensors* **20**(17), 4745 (2020).
37. Vafapour, Z. Polarization-independent perfect optical metamaterial absorber as a glucose sensor in food industry applications. *IEEE Trans. Nanobiosci.* **18**(4), 622–627 (2019).

38. Vafapour, Z. et al. The potential of refractive index nanobiosensing using a multi-band optically tuned perfect light metamaterial absorber. *IEEE Sens. J.* **21**(12), 13786–13793 (2021).

Author contributions
all authors contributed equally to this work.

Declarations

Competing interests
The authors declare no competing interests.

Additional information
Correspondence and requests for materials should be addressed to H.H.